Supporting Information

Sugiyama et al. 10.1073/pnas.0903186107

SI Text

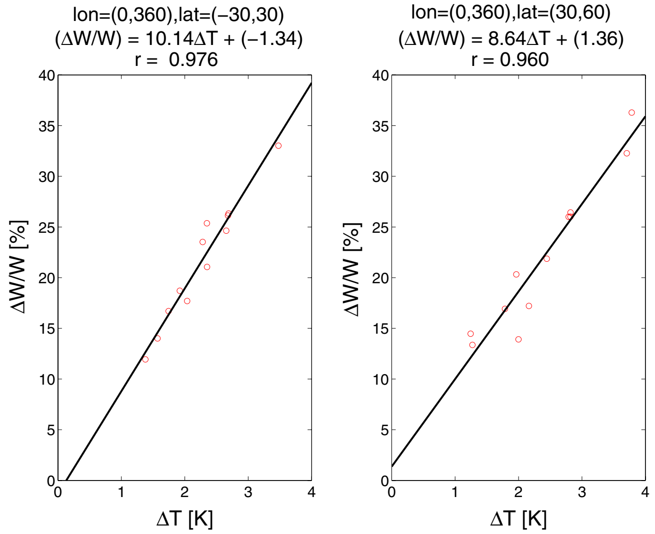

Fig. S1. Scatter plots of the fractional change in climatological-mean precipitable water and the change in temperature for (*Left*) the tropics and (*Right*) the midlatitudes for MIROC and the CMIP3 models. Shown at the top of each panel is the result of a least-squares fit. Precipitable water increases differ from the oft-quoted number of 7%/K in most cases, which is more representative of the lower troposphere than the entire troposphere.

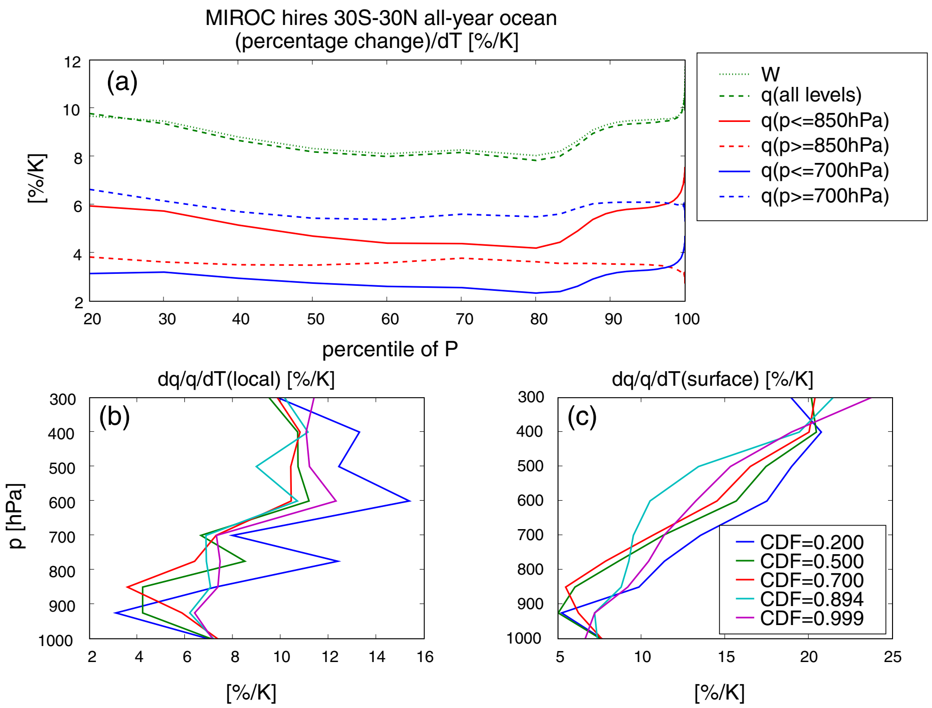

Fig. S2. Decomposition of the change in precipitable water by pressure levels in MIROC. (*a*) shows the fractional change in precipitable water *W* and the change in the specific humidity vertically integrated over various levels, normalized by that integrated over the entire troposphere. For example, "q (p≤850hPa)" refers to $\Delta(\int_0^{850} qdp)/(\int_0^{1000} qdp)$ and "q(p≥850hPa)," $\Delta(\int_{850}^{1000} qdp)/(\int_0^{1000} qdp)$ so that the two lines denoted by "q(p≤850hPa)" and "q (p≥850hPa)" add up to the "q(all levels)". The display format is similar to that in Fig. 3, except that the horizontal axis is linear in the percentile of precipitation. "q(all levels)" differs from *W* slightly, and the difference is because the vertical integration is performed over a non-native, coarse pressure grid. In spite of its relative small contribution to the overall precipitable water, the change in the upper troposphere characterizes the shape of the *W* change distribution over the precipitation percentile, particularly for the very high percentiles. (*b*) and (*c*) describe the fractional change in specific humidity at each pressure level normalized by local temperature (*b*) and the area-averaged surface temperature (*c*) for various percentiles of precipitation (see the legend of *c*). The fractional change in specific humidity normalized by local temperature is about $7\%/K$ near the surface, and increases up to ~$12\%/K$ above the freezing level (~500 hPa) owing to the temperature dependence of the Clausius–Clapeyron relationship. Furthermore, it becomes much larger when normalized by the surface temperature because of the reduction in the temperature lapse rate.

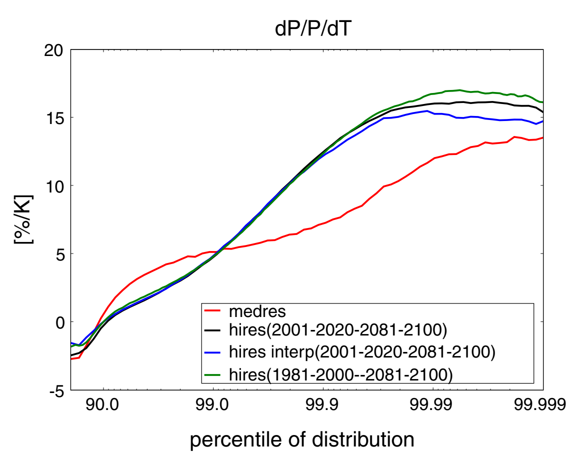

Fig. S3. Comparisons of the resolutions and analysis periods (both indicated in the legend) with respect to fractional changes in precipitation per unit warming for MIROC. "hires interp" indicates the high-resolution version outputs bilinearly interpolated onto the medium-resolution grid. The difference between the medium-resolution version and the three curves from the high-resolution version (including the interpolated one) is generally larger than the difference among different curves of the high-resolution version. Notice also that different binning schemes are applied to different "hires" curves. There are 200 bins for 0–1000 mm/day for "hires (1981-200–2081-2100)" and 100 bins for 0–400 mm/day for "hires (2001-2020–2081-2100)" and "hires interp". The fractional changes in precipitation are not sensitive to this difference.

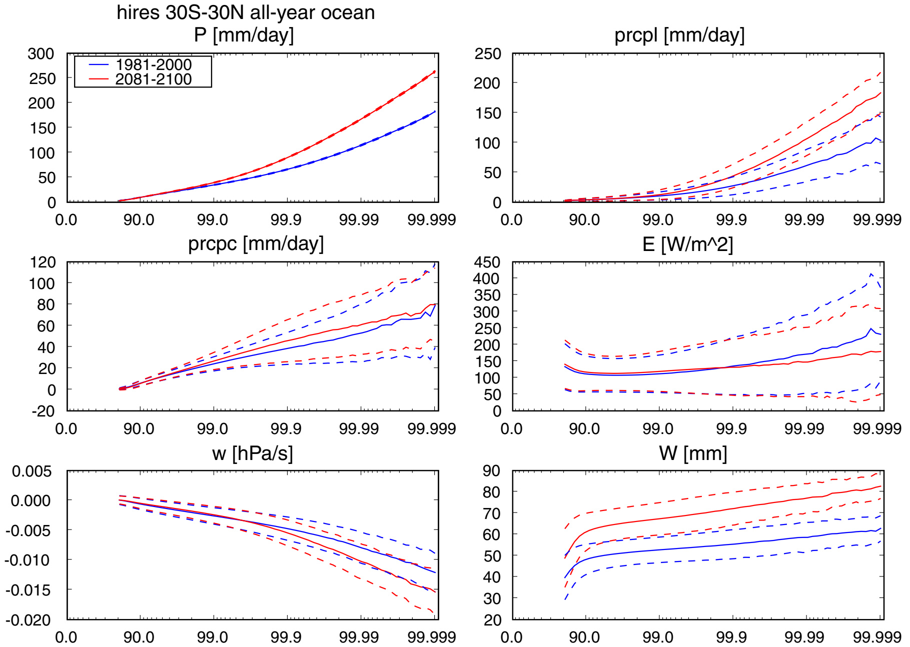

Fig. S4. Mean values and standard deviations of the variables conditioned on precipitation extremes in MIROC, which correspond to the results shown in Fig. 3. Plotted are: precipitation *P*, large-scale precipitation prcpl, convective precipitation prcpc, evaporation *E*, the pressure velocity at the 500 hPa level *w*, and precipitable water *W*. The solid lines denote the mean values and the dashed lines represent a one-standard-deviation range. The standard deviation of precipitation *P* is barely visible because of the relatively small bin size used. Although the errors are large, the increases for extreme events are as large as, or larger than, one standard deviation for large-scale precipitation, precipitable water, and the mid-level vertical motion.

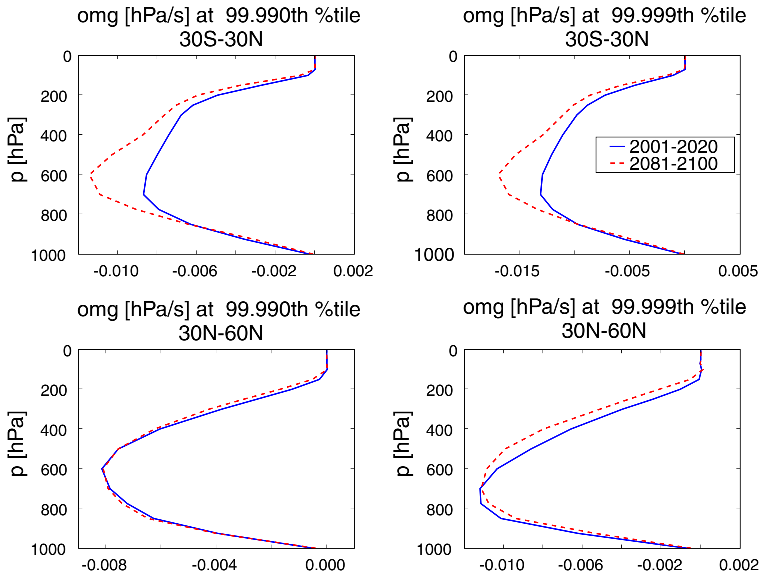

Fig. S5. Mean vertical motion conditioned on precipitation extremes in MIROC. The upper two panels represent 30°S–60°N, all seasons, whereas the lower panels 30–60°N, December-January-February. The text above each panel describes the percentile of precipitation distribution for which the composite has been constructed. The profile of vertical motion shifts upward under global warming.

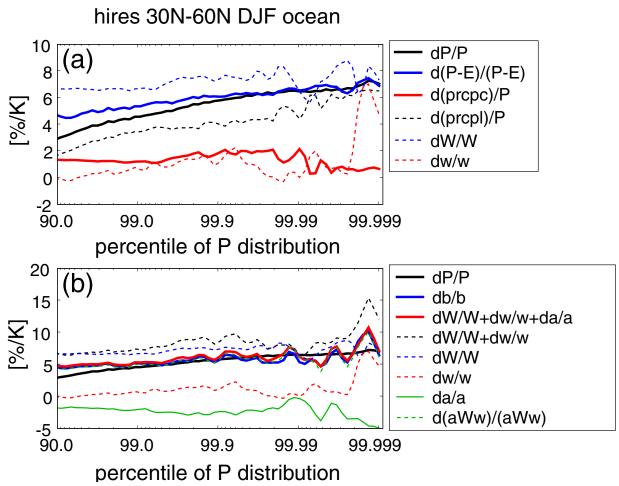

Fig. S6. As in Fig. 3 but for 30–60°N, the boreal winter (December-January-February) in MIROC.

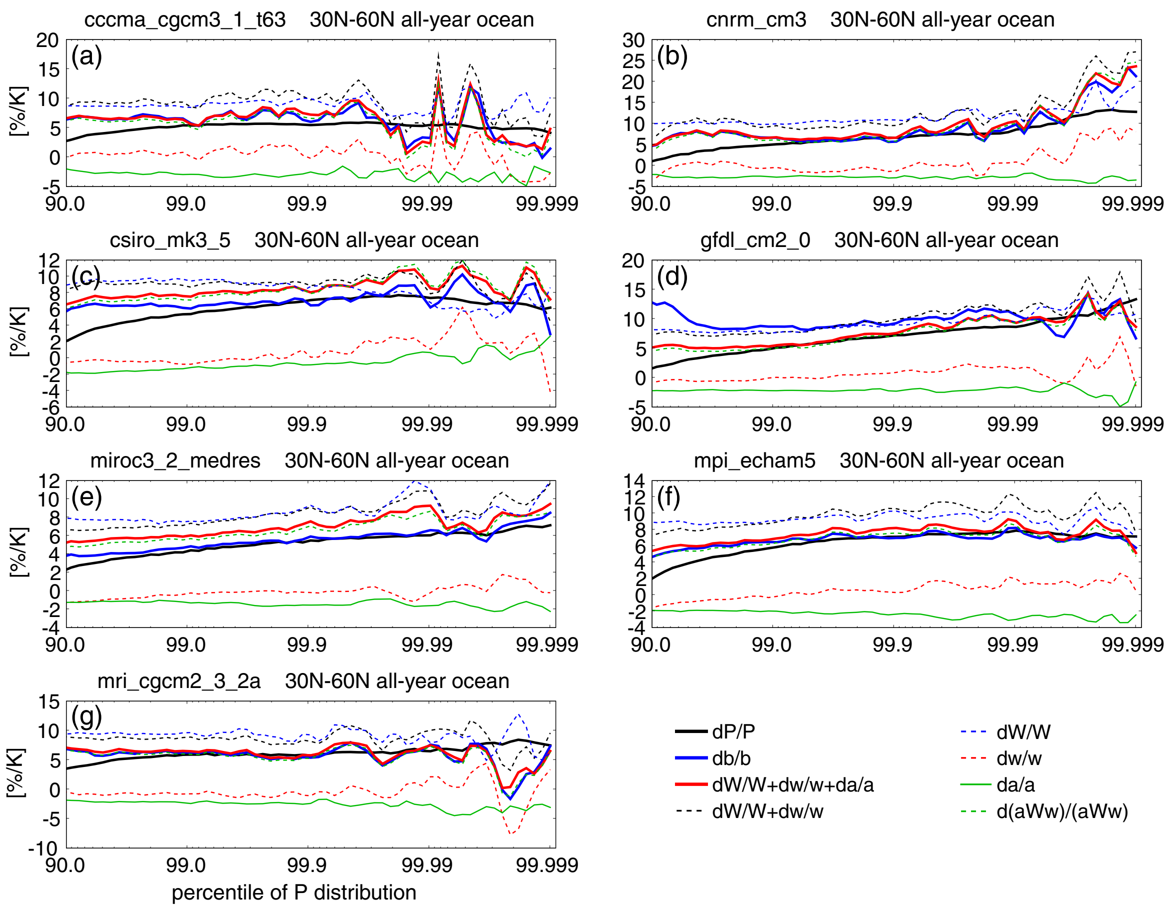

Fig. S7. Decomposition of precipitation extremes in the CMIP3 models. As in Fig. 4 but for 30–60°N.

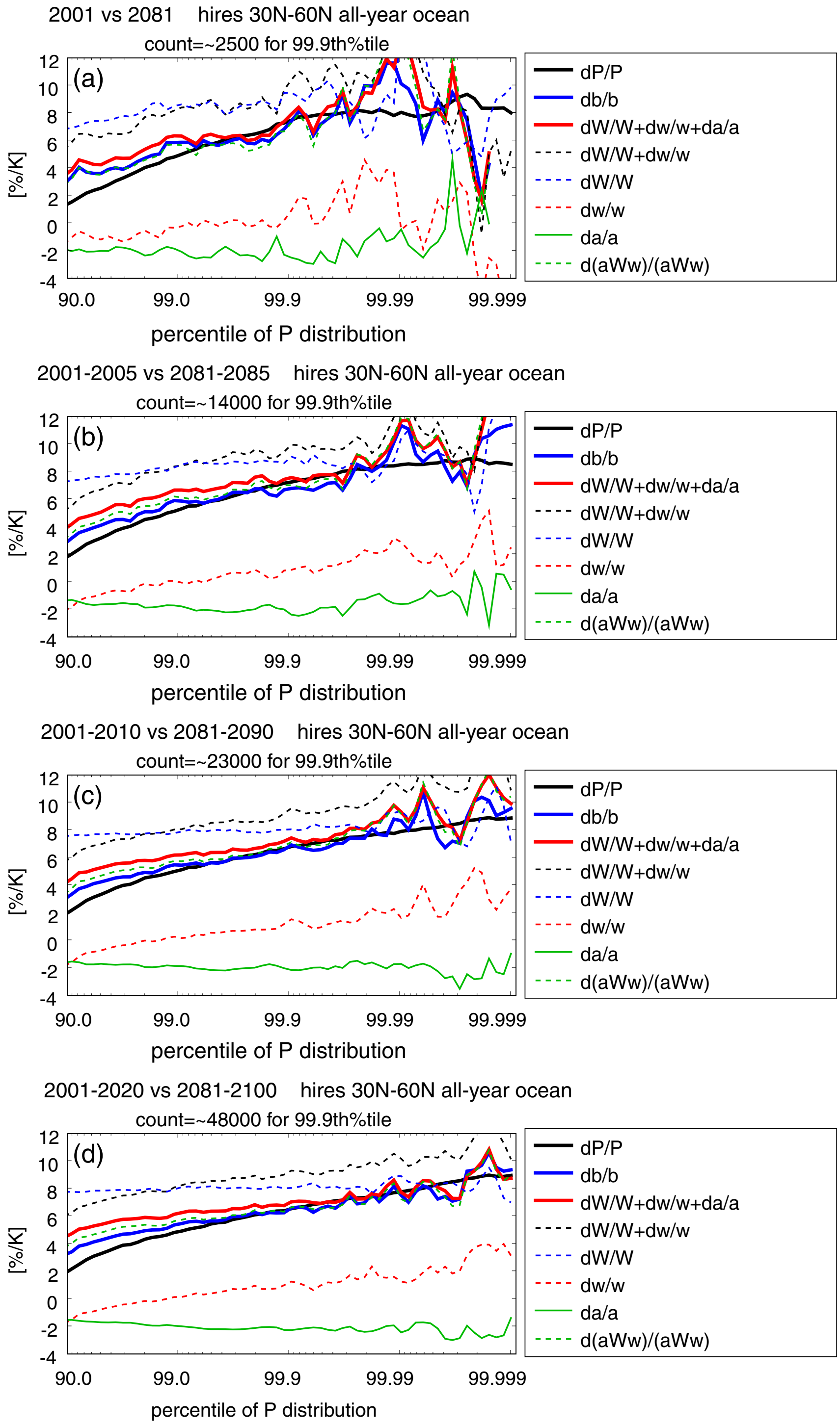

Fig. S8. Noise and the sample size in MIROC. Each panel is in the same format as Fig. 3*B*, but the period used for each panel is varied in order to assess how the sample size affects the noise. The count of the events that exceed the 99.9th percentile level of precipitation is shown at the top of each panel. The noise (wiggles) decreases with the sample size.